Tao controls epithelial morphogenesis by promoting Fasciclin 2 endocytosis

Juan Manuel Gomez, Ying Wang, and Veit Riechmann

Department of Cell and Molecular Biology, Medical Faculty Mannheim, Heidelberg University, D-68167 Mannheim, Germany

Regulation of epithelial cell shape, for example, changes in relative sizes of apical, basal, and lateral membranes, is a key mechanism driving morphogenesis. However, it is unclear how epithelial cells control the size of their membranes. In the epithelium of the *Drosophila melanogaster* ovary, cuboidal precursor cells transform into a squamous epithelium through a process that involves lateral membrane shortening coupled to apical membrane extension. In this paper, we report a mutation in the gene *Tao*, which resulted in the loss of this cuboidal to squamous transition. We show that the inability of *Tao* mutant cells to shorten their membranes was caused by the accumulation of the cell adhesion molecule Fasciclin 2, the *Drosophila* N-CAM (neural cell adhesion molecule) homologue. Fasciclin 2 accumulation at the lateral membrane of *Tao* mutant cells prevented membrane shrinking and thereby inhibited morphogenesis. In wild-type cells, *Tao* initiated morphogenesis by promoting Fasciclin 2 endocytosis at the lateral membrane. Thus, we identify here a mechanism controlling the morphogenesis of a squamous epithelium.

Introduction

Relative changes in the dimensions of apical, lateral, and basal membranes control various morphogenesis processes (St Johnston and Sanson, 2011). For example, the constriction of the apical membrane in a group of epithelial cells leads to their invagination, a mechanism that is used in diverse developmental programs, such as *Drosophila melanogaster* gastrulation or neural tube formation in vertebrates. Although we are beginning to understand the molecular machinery controlling apical constriction (Harris, 2012; Levayer and Lecuit, 2012), it remains unclear how the formation of squamous and columnar epithelia is regulated.

Morphogenesis of a columnar epithelium from cuboidal precursors involves the expansion of the lateral membrane. In contrast, formation of squamous epithelia requires shrinking of the lateral membrane and expansion of the apical and basal membranes. It is unclear how these changes in membrane size and cell shape are regulated. Previous studies suggest roles for cell junctions and the cytoskeleton. It has been shown that the reorganization of the microtubule cytoskeleton is involved in the stretching of the *Drosophila* amnioserosa (Pope and Harris, 2008). A potential role of actin–Myosin-based contractility in preventing cell stretching can be deduced from data in the *Drosophila* follicular epithelium, where cells lacking Myosin function undergo a transition from a cuboidal to squamous cell shape (Wang and Riechmann, 2007). The same phenotype was observed when the function of adherens junctions is disturbed (Müller, 2000; Tanentzapf et al., 2000). The finding that compromised cell adhesion results in cell flattening suggests that squamous cell morphogenesis can be induced by reducing adhesion between cells. This raises the possibility that epithelial cells control the size of their lateral membrane by regulating the abundance or localization of cell adhesion molecules. An increase in the number of adhesion molecules could lead to an expansion of the lateral membrane, whereas their reduction allows membrane shrinking.

Two important protein families mediating cell adhesion are cadherins and immunoglobulin superfamily of cell adhesion molecules. A prominent member of the latter family is N-CAM (neural cell adhesion molecule) and its insect homologue Fas2 (Fasciclin 2), which mediate homophilic interactions in the

Correspondence to Veit Riechmann: veit.riechmann@medma.uni-heidelberg.de

Y. Wang's present address is Dept. of Molecular and Cellular Biology, Baylor College of Medicine, Houston, TX 77030.

Abbreviations used in this paper: aPKC, atypical PKC; Arm, Armadillo; Crb, Crumbs; Dlg, Discs large; EMS, ethane methyl sulfonate; Eya, Eyes absent; FRT, FLP recombination target; PNS, peripheral nervous system; SWH, Salvador–Warts–Hippo; UAS, upstream activation sequence.

The Rockefeller University Press $30.00
J. Cell Biol. Vol. 199 No. 7 1131–1143
www.jcb.org/cgi/doi/10.1083/jcb.201207150

extracellular space. E-cadherin is a central component of the adherens junctions, the site of apicolateral cell contacts. The extracellular part of E-cadherin connects neighboring cells, whereas its intracellular part serves as an anchoring point for the actin cytoskeleton and several other proteins, including β-Catenin (Harris and Tepass, 2010; Baum and Georgiou, 2011).

Epithelial morphogenesis can be studied in the follicular epithelium of the *Drosophila* ovary. This organ is composed of follicles of different ages, which are subdivided into 14 different developmental stages (Horne-Badovinac and Bilder, 2005). Follicles or egg chambers consist of an inner cyst of germline cells (made of 15 nurse cells and one oocyte) surrounded by a monolayered follicular epithelium with initially cuboidal-shaped cells (Fig. S1 A). During early oogenesis, the germline cyst grows in size, leading to a volume increase that is accommodated by cell divisions in the epithelium. This changes after stage 6 when cell divisions cease because of the expression of Delta in the germline activating Notch signaling in the epithelium (Deng et al., 2001; López-Schier and St Johnston, 2001). Although the germline cyst continues to increase its volume after stage 6, the epithelium undergoes morphogenesis and subdivides into an anterior squamous and a posterior columnar part (Fig. S1 B). As a result, egg chambers develop with a posterior columnar epithelium covering the oocyte and an anterior squamous epithelium consisting of large and flat cells covering the nurse cells.

Morphometric analysis and mechanical modeling suggest that the growth of the inner cyst is a critical force for the morphogenesis of the squamous epithelium. Kolahi et al. (2009) propose a model in which the volume increase of the inner cyst exerts a tensile force on the outer epithelium inducing flattening of cells specifically in anterior epithelium. In the posterior epithelium, this force is counteracted by the apical actin cytoskeleton, which is organized by β-Spectrin and contracted by Myosin (Zarnescu and Thomas, 1999; Wang and Riechmann, 2007). Anterior cells are unable to counteract cyst pressure and flatten. A possible reason for their inability to resist pressure is the locally restricted disassembly of their adherens junctions at positions where three or four cells meet (Grammont, 2007). As the adherens junctions anchor the actin cytoskeleton, their local breakdown could destabilize the apical actin network and trigger cell flattening (Kolahi et al., 2009). Adherens junction disassembly proceeds from anterior to the middle region of the follicle concomitant with stretching, suggesting a critical role for squamous cell morphogenesis (Grammont, 2007). It has been shown that Notch signaling is required for adherens junction breakdown during stretching (Grammont, 2007), but other genes contributing to epithelial stretching are unknown. Here, we identify the gene *Tao* as a critical regulator for squamous cell morphogenesis.

The Ser/Thr kinase Tao has been shown to activate the stress-responsive MAPK pathway in mammalian cell lines (Hutchison et al., 1998; Raman et al., 2007). Tao uses the same pathway in cultured hippocampal neurons to trigger endocytosis of N-cadherin in dendritic spines (Yasuda et al., 2007). A biochemical study isolated Tao because of its ability to phosphorylate Par-1, a kinase regulating microtubule dynamics and cell polarity (Timm et al., 2003). Analysis of *Tao* in *Drosophila* revealed functions in controlling microtubule plus-end growth in cultured cells (Liu et al., 2010), in regulating apoptosis of germ cells in the embryo (Sato et al., 2007), and in the development of the adult brain (King et al., 2011). Two recent studies show that Tao is also involved in growth regulation of imaginal discs, in which Tao activates the Salvador–Warts–Hippo (SWH) pathway by phosphorylating Hippo kinase (Boggiano et al., 2011; Poon et al., 2011). Here, we report the generation of a *Tao* allele lacking kinase activity, which allowed us to study a new function of *Tao* in regulating morphogenesis of the follicular epithelium. *Tao* reduces lateral adhesion between epithelial cells by promoting Fas2 endocytosis. Decreased cell adhesion permits shrinking of the lateral membrane and initiates the morphogenesis of the squamous epithelium.

Results

Tao is required for follicle cell morphogenesis

We have identified Tao protein in a biochemical screen for proteins that are phosphorylated by Par-1 (Riechmann and Ephrussi, 2004). To identify a possible function of Tao during *Drosophila* oogenesis, we performed an ethane methyl sulfonate (EMS) screen, in which we generated one chromosome with a point mutation in the second exon of the *Tao* gene (Tao^{eta}), resulting in a premature stop codon at aa 64. The predicted protein harbors only a 37-aa fragment of the kinase domain lacking its active site. As homozygous Tao^{eta} mutants are lethal, we recombined the mutation onto a FLP recombination target (FRT) chromosome to generate genetic mosaics with the FRT/FLP technique (Xu and Rubin, 1993). Par-1 controls the establishment of the anterior–posterior axis of the oocyte by polarizing the microtubule cytoskeleton, which is necessary for the localization of Oskar to the posterior pole of the oocyte (Shulman et al., 2000; Tomancak et al., 2000). Surprisingly, neither Oskar localization nor microtubule polarity is affected in *Tao* mutant oocytes, indicating that *Tao* is not necessary for establishment of anterior–posterior polarity (Fig. S2 A).

Closer inspection of egg chambers with Tao^{eta} mutant cells revealed morphological defects in the follicular epithelium, which become apparent during stage 8/9 when a monolayer of cuboidal precursors is transformed into a squamous anterior and a columnar posterior epithelium. *Tao* mutant cell clones in the anterior part of the epithelium fail to stretch and stay cuboidal (Fig. 1 A, left clone). Posterior clones show milder morphological defects, which are reflected by an increase in the length of the lateral membrane compared with wild-type cells (Fig. 1 A, right clone). To test whether Tao^{eta} behaves as a loss-of-function allele, we generated a chromosome with a small deletion that uncovers the entire open reading frame of *Tao* and two neighboring genes (see Materials and methods). Cell clones generated with this deletion show the same epithelial defects as Tao^{eta} clones, indicating that Tao^{eta} is indeed a loss-of-function allele (Fig. 1 B).

To confirm that the morphogenesis defect is caused by loss of *Tao* function, we performed rescue experiments with

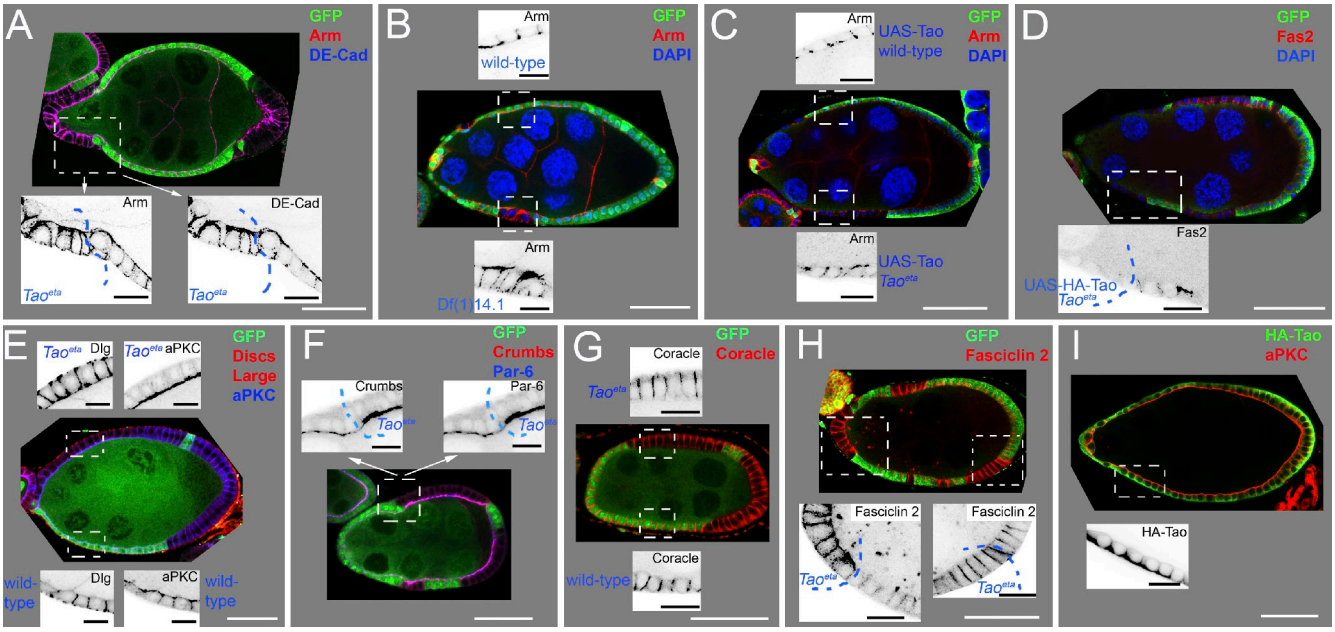

Figure 1. ***Tao* regulates epithelial cell shape and accumulation of membrane proteins.** Egg chambers are shown harboring homozygous *Tao* mutant cell clones, which are marked by the absence of GFP. Follicles are stained with the indicated markers. Insets show enlarged areas of the region marked by the white frame. Blue dotted lines mark the border of the Tao mutant clones. (A–D) Stage 9 egg chambers. (A) Follicle with two *Tao* mutant cell clones in the anterior and posterior epithelium showing elongated epithelial cells and overaccumulation of Arm and DE-cadherin (DE-Cad). (B) Cell clones homozygously mutant for a deletion uncovering the open reading frame of the *Tao* gene (Df(1)14.1) showing elongated lateral membranes and overaccumulation of Arm. The bottom inset shows a magnified area of mutant cells, and the top inset shows wild-type cells for comparison. (C) Egg chamber in which the stretching defect and Arm accumulation in the anterior epithelium is rescued by expression of a *GR1-Gal4*–driven *UAS-Tao* transgene. (D) Rescue of the *Tao* stretching defect with a *GR1-Gal4*–driven *UAS-HA-Tao* transgene. On the left side of the inset, a Tao^{eta} mutant clone is shown, which is rescued by Gal4-driven *Tao* expression. Note that cells stretch and that Fas2 is not detectable. (E–H) Stage 8 egg chambers. (E) *Tao* mutant cell clones showing the increased accumulation of aPKC at the apical membrane (right insets). Levels of Dlg protein at the lateral membrane show no obvious increase (left insets). *Tao* mutant cells (top insets) have an elongated apical–basal axis. (F) *Tao* mutant cell clones showing overaccumulation of Crb and Par-6 proteins at the apical membrane. (G) *Tao* mutant cell clones showing an elongated apical–basal axis and expressing normal levels of the lateral membrane marker Coracle. (H) *Tao* mutant cells show a strong increase of Fas2 at the lateral membrane. (I) Expression of the *UAS-HA-Tao* transgene in an otherwise wild-type background showing the localization of Tao protein at the lateral membrane and in the basolateral cytoplasm. Processing of the images involved adjustment of γ settings. Bars: (white) 50 µm; (black) 12.5 µm.

an *upstream activation sequence* (*UAS*)-*Tao* transgene, which rescues lethality of homozygous Tao^{eta} mutants when induced by the ubiquitous *Tubulin-Gal4* driver line. The same transgene is able to fully rescue the stretching process in the anterior epithelial cells with a follicle cell–specific driver (*GR1-Gal4*; Fig. 1 C). We analyzed the subcellular localization of Tao by expressing a HA fusion protein, which also rescues morphogenesis (Fig. 1 D). HA-Tao protein accumulates in the basolateral cytoplasm and at the lateral membrane of the follicular epithelium (Fig. 1 I).

Tao regulates accumulation of polarity proteins at the plasma membrane

We tested whether *Tao* controls epithelial morphogenesis by one of its known mechanism or pathways. It has been shown that *Tao* regulates the SWH pathway in imaginal discs (Meignin et al., 2007; Polesello and Tapon, 2007). In the follicular epithelium, SWH signaling is involved in ceasing cell proliferation after stage 6 of oogenesis, and cell clones with loss of SWH activity show prolonged proliferation as well as aberrant localization and delayed down-regulation of Notch. Moreover, SWH mutant clones express Fasciclin 3 and Eyes absent (Eya) ectopically after stage 6. Homozygous Tao^{eta} clones, however, reveal a normal localization of Notch, Fasciclin 3, and Eya and show no cell proliferation after stage 6 as detected by phospho–Histone H3 stainings ($n = 51$; Fig. S2, B–E). We therefore conclude that *Tao* is not acting via the SWH pathway in the follicular epithelium. We also ruled out that the morphogenesis defects in *Tao* mutant cells results from patterning defects in the follicular epithelium by analyzing the localization of the cell fate specification markers Eya and phospho-Mad (Fig. S2, F–I).

In mammalian cell lines, Tao activates the p38 signaling cascade in response to cellular stress (Hutchison et al., 1998; Raman et al., 2007). To test whether this signaling module is activated by Tao in the follicular epithelium, we analyzed the function of five kinases that were shown to act downstream of Tao. Neither cell clones for *Mpk2D/p38a* and *Dsor* nor double mutant clones for *licorne* and *hemipterous* showed defects in follicle cell morphology (Fig. S2, J–L). Moreover, expression of a dominant-negative form of p38b in the follicular epithelium did not produce defects in the follicular epithelium (unpublished data). These data suggest that *Tao* is unlikely to regulate morphogenesis by activating the p38 cascade.

As *Tao* regulates microtubule dynamics in mammalian and *Drosophila* cell lines (Timm et al., 2003; Liu et al., 2010), we examined whether *Tao* controls epithelial cell shape by acting on the cytoskeleton. Careful analysis of the microtubule cytoskeleton showed no differences in the organization of

microtubules between wild-type and *Tao* mutant cells. Neither the density of α-Tubulin–stained microtubules nor microtubule polarity revealed by the localization of γ-Tubulin, Nod-lacZ, and Kinesin-lacZ is affected in *Tao* mutant cells (Fig. S3, A–D). Moreover, *Tao* mutant cells do not show significant differences in the distribution of F-actin, α-Spectrin, and Myosin activity, indicating that *Tao* does not act on the actin cytoskeleton (Fig. S3, E and F). We therefore conclude that *Tao* does not regulate morphogenesis via the cytoskeleton.

To examine a possible role of Tao in cell polarity, we analyzed epithelial membrane domains, which are established by polarity proteins localizing to the apical or lateral membrane. Crumbs (Crb), Par-6, and atypical PKC (aPKC) localize to the apical membrane, whereas Discs large (Dlg), Coracle, and Fas2 distribute laterally (Laprise and Tepass, 2011). *Tao* mutant follicle cells localize all aforementioned proteins correctly, indicating that the overall apicobasal polarity of the follicular epithelium is not affected (Fig. 1, E–H). Analysis of the adherens junction components DE-cadherin and β-Catenin/Armadillo (Arm) revealed that they are present in the apicolateral region of the epithelium but accumulate at higher levels compared with neighboring wild-type cells (Figs. 1 A and 2 A). Moreover, their localization is not restricted to the apicolateral region but spreads into the apical membrane domain of *Tao* mutant cells. The apical marker Crb, Par-6, and aPKC also accumulate at higher levels but are still restricted to their domain (Fig. 1, E and F). Among the lateral markers, only Fas2 shows an increased membrane accumulation, whereas we detected no obvious difference in Dlg and Coracle levels (Fig. 1, E, G, and H). Thus, although *Tao* is not essential for the establishment of membrane polarity, it regulates the accumulation proteins at the plasma membrane.

Fas2 suppresses epithelial morphogenesis defects in *Tao* mutant cells

To assess whether the increased accumulation of membrane proteins causes the morphogenesis defects in *Tao* mutant cells, we tested whether a reduction of this accumulation by RNAi rescues *Tao* defects. To identify possible mediators of the defects, we performed a candidate in vivo RNAi interaction screen. We generated *Tao* mutant cell clones, in which candidate proteins are knocked down by inducing UAS-RNAi and UAS-Flippase transgenes with the same Gal4 driver line (see Materials and methods). In this screen, we included not only proteins that accumulate in *Tao* mutant cells but also other possible *Tao*-interacting genes, such as *par-1* and *Eb1* (encoding a microtubule plus end–binding protein), and genes encoding members of the SWH pathway (Table S1).

Fig. 2 compares the results for the interaction of *Tao* with genes encoding the transmembrane proteins *Crb*, *DE-cadherin*, and *Fas2* as examples. Among the 10 genes tested in this approach, only *Fas2* RNAi rescues *Tao* morphogenesis defects. In approximately half of the analyzed stage 9 egg chambers, the stretching defects of *Tao* mutant cell clones ($n = 16$) were clearly suppressed when *Fas2* function was simultaneously reduced by RNAi. Analysis of Fas2 expression in this experiment revealed residual protein after RNAi, indicating an incomplete knockdown and providing an explanation why the rescue is not fully penetrant (Fig. 2 H, inset).

To quantify the results of the interaction screen, we measured the length of the apicobasal axis of anterior epithelial cells to calculate a mean apicobasal length proportion (see Fig. S4). The mean value for wild-type versus *Tao* mutant cells is 1.8, meaning that the mean apicobasal axis of anterior *Tao* mutant cells is almost twice as long. This is in contrast to the mean value of 1.2 measured in egg chambers, in which *Tao* mutant clones and *Fas2* knockdown have been induced. Thus, a reduction of Fas2 protein levels suppresses the morphogenetic defects of *Tao* mutant cells. Interestingly, *Fas2* knockdown in *Tao* mutant cells suppresses not only the morphological defects but also the overaccumulation of Arm at the membrane (Fig. 2 D). As no other gene knockdown in our candidate approach was able to suppress *Tao* defects, we conclude that the overaccumulation of Fas2 protein in *Tao* cells is a major reason for their inability to undergo morphogenesis.

To further support that Fas2 accumulation is causing *Tao* morphogenesis defects, we generated *Fas2 Tao* double mutants by recombining a null allele ($Fas2^{eb1112}$) with Tao^{eta}. Larger homozygous mutant cell clones in the follicular epithelium are lethal, suggesting an interaction of the two genes in cell viability during early oogenesis. However, we could recover small clones in stage 8/9 egg chambers, which all stretch normally ($n = 8$; Fig. 2, I and J). Moreover, double mutant clones accumulate normal Arm protein levels at their membranes, indicating a complete rescue of the *Tao* phenotype. Thus, *Fas2 Tao* double mutant clones strongly support that the morphogenesis defects in *Tao* mutant cells are caused by Fas2 accumulation. We therefore hypothesized that *Tao* acts through Fas2 during epithelial morphogenesis.

Timely controlled down-regulation of Fas2 is critical for epithelial stretching

The transmembrane protein Fas2 harbors five immunoglobulin domains, which mediate homophilic cell adhesion between the lateral membranes of follicle cells (Szafranski and Goode, 2004). The homophilic adhesion properties of Fas2 suggest a simple explanation for the stretching failure of *Tao* mutant cells: the increased accumulation of Fas2 at the lateral membrane results in increased cell–cell adhesion, which prevents membrane shrinking and hence morphogenesis. As this hypothesis implies that Fas2 is lost from the lateral membrane before stretching, we reexamined Fas2 localization during morphogenesis. It has been reported that the Fas2 protein is absent from anterior follicle cells at stage 8 (Szafranski and Goode, 2004). Our analysis of the temporal changes in Fas2 localization showed that anterior epithelial cells loose Fas2 when they are still cuboidal, indicating that down-regulation precedes stretching (Fig. 3 B). This supports the idea that Fas2 has to be removed from the lateral membrane to allow stretching. Fas2 is no longer detectable in stretching follicle cells (Fig. 3, C–D′), whereas DE-cadherin forms a zonula adherens (Fig. 3 D, red channel). This suggests that cell adhesion in stretching cells is mainly mediated by DE-cadherin. In contrast to the anterior cells, posterior cells maintain Fas2 at their

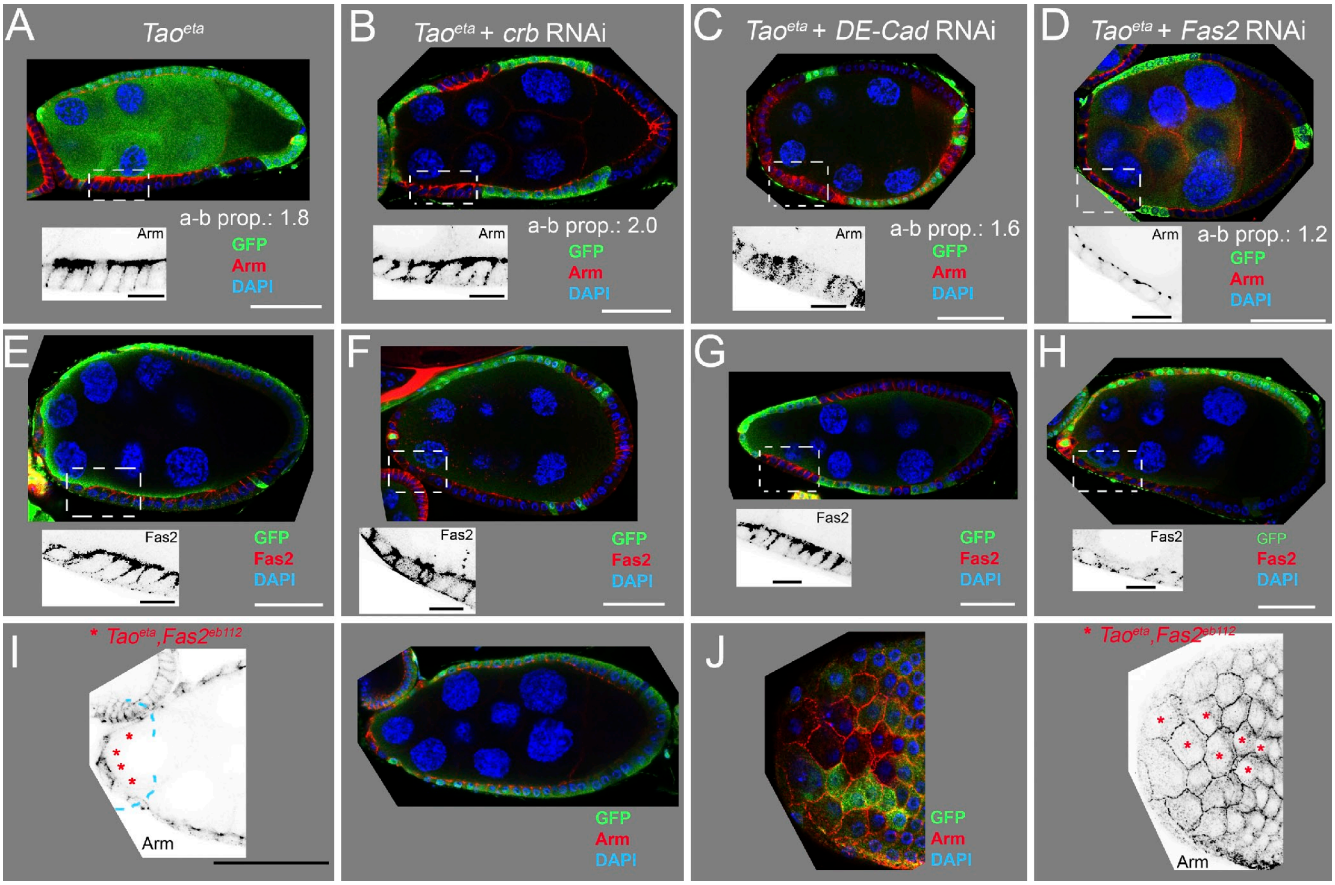

Figure 2. **Morphogenesis defects in *Tao* mutant cells are mediated by Fas2 overaccumulation.** (A–I) Stage 9 egg chambers. Insets show enlarged areas of the region marked by the white frames. (A–H) Egg chambers with *Tao* mutant clones marked by the absence of GFP and stained for Arm (A–D) or Fas2 (E–H). The indicated apical–basal length proportions (a-b prop.; see also Fig. S4) is the mean value obtained in at least three different asymmetric clones. A and E show *Tao* clones in a wild-type background, and B, C, and F–H show clones in follicles in which *crb*, *DE-cadherin* (*DE-Cad*), and *Fas2* are knocked down using *GR1-Gal4*–driven UAS-inverted repeat transgenes. (B and F) *crb* knockdown neither suppresses the stretching defects nor the overaccumulation of Arm and Fas2 in *Tao* clones. (C and G) *DE-cadherin* knockdown results in defects in egg chamber morphology and mislocalization of Arm, which are explained by defects in zonula adherens formation. Fas2 accumulates at the lateral membrane of *Tao* mutant cells, which fail to stretch. (D and H) *Fas2* knockdown suppresses the stretching defects in *Tao* mutant cells, and Arm accumulation reverts to normal levels. Note that the residual Fas2 protein is detectable, indicating that the knockdown is not complete (inset in H). (I and J) Follicles with cell clones doubly mutant for *Tao* and *Fas2* stained for Arm protein. Images to the right of I and J show the Arm channel alone. Mutant cells are marked by red asterisks and reveal no stretching defects. J (left) shows an optical confocal section at the level of the zonula adherens, revealing the onset of stretching in the anterior-most cells. Arm overaccumulation is suppressed. Eight double mutant clones were obtained in total, two of them were in an asymmetric position (not depicted), allowing the calculation of the apical–basal length proportion with a value of 1.1. Blue dotted lines mark the border of the Tao mutant clones. Processing of the images involved adjustment of γ settings. Bars: (white) 50 µm; (black) 12.5 µm.

membranes, where it is now confined to the apicolateral region (Fig. 3 C, arrowheads).

To test the hypothesis that Fas2 interferes with stretching of anterior cells, we overexpressed a *UAS-Fas2-YFP* construct using *traffic jam-Gal4*, a driver line providing high expression levels in all follicle cells. Fas2 overexpression delays stretching and results in the formation of elongated egg chambers, in which anterior follicle cells retain a cuboidal cell shape at stage 9 (Fig. 3 E). Interestingly, these cell shape defects are accompanied by increased levels of the adherens junction component Arm at the apical membrane closely resembling *Tao* mutant cells (Figs. 3 E and 2 A, compare insets). Thus, Fas2 overexpression mimics the *Tao* phenotype, strongly supporting the hypothesis that increased Fas2 levels cause the defects of *Tao* mutant cells. In summary, our data show that Fas2 is lost from anterior follicle cells before they undergo stretching and that prolonged Fas2 expression interferes with lateral membrane shrinking. Thus, timely controlled removal of Fas2 is critical for stretching of the anterior follicle cells.

The critical role for Fas2 in epithelial morphogenesis raised the question whether the adhesion molecule is required for cell shape maintenance before stretching starts. Analysis of *Fas2* mutant cell clones showed that they stay cuboidal until stage 7 and then undergo normal morphogenesis (Fig. 3, F and G). Thus, although the down-regulation of Fas2 is critical for stretching, the protein is not essential for maintaining epithelial cell shape before morphogenesis.

Fas2 removal from the lateral membrane is mediated by endocytosis

Fas2 down-regulation in the follicular epithelium is controlled at the transcriptional level (Szafranski and Goode, 2004). We confirmed this by analyzing three enhancer trap lines, which reflect the transcriptional activity of the Fas2 locus (Fig. S5, A–C;

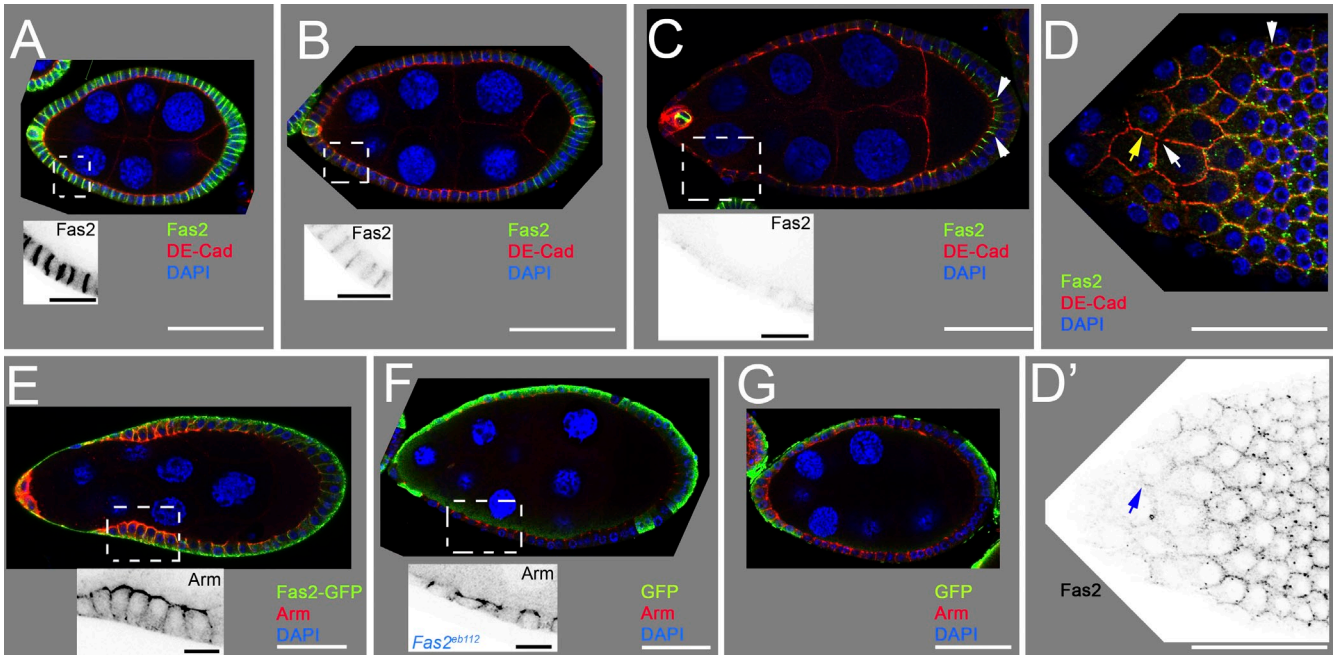

Figure 3. **The role of Fas2 during morphogenesis of the squamous epithelium.** (A–D) Localization of Fas2 and DE-cadherin (DE-Cad) in stage 7 (A), stage 8 (B), and stage 9 (C and D) follicles. Insets show the Fas2 signal in the framed regions at a higher magnification. Fas2 is down-regulated in anterior follicle cells between stages 7 and 8. (B) Note the disappearance of the Fas2 signal when the cells are still cuboidal. (C) Arrowheads show Fas2 signal in the apicolateral region of the posterior epithelium. (D) Surface view of the anterior epithelium during stretching. DE-cadherin highlights the zonula adherens, which is continuous at two cell borders (yellow arrow) and which disassembles at the four cell border (white arrow). White arrowhead marks a Fas2 puncta in the cytoplasm. D′ shows the Fas2 channel alone. Fas2 is no longer detectable at the membrane of the anterior follicle cells (arrow) and appears in puncta in more posterior cells. (E) Stage 9 egg chamber in which a *UAS-Fas2-YFP* transgene is overexpressed. Only the anterior-most follicle cells flatten, whereas the remaining anterior cells retain a cuboidal shape. Egg chamber morphology is affected as revealed by the elongated shape of the follicle (compare with stage 9 follicles in C and F). The inset shows the accumulation of Arm at the apical membrane. (F and G) Follicle cell clones mutant for the null allele $Fas2^{eb1112}$ marked by the absence of GFP. Mutant cells show no shape defects before (G) and during (F) morphogenesis. Processing of the images involved adjustment of γ settings. Bars: (white) 50 µm; (black) 12.5 µm.

and not depicted). To examine whether *Tao* is involved in Fas2 repression, we recombined the enhancer trap insertions with the Tao^{eta} mutation and induced mutant cell clones. A comparison of reporter signal intensities between mutant and heterozygous cells provided no evidence for a function of *Tao* in repressing Fas2 transcription (Table S2 and Fig. S5, D and E). Thus, *Tao* does not appear to regulate Fas2 gene expression and might mediate down-regulation of Fas2 at a posttranscriptional level.

A possible level of control is the removal of existing protein from the lateral membrane, which is most commonly achieved by packaging the protein into vesicles that are destined for degradation. To investigate the role of vesicle trafficking, we analyzed Fas2 distribution in optical sections perpendicular to the apicobasal axis of the epithelium and identified cytoplasmic Fas2-positive puncta (Figs. 4 A and 3 D′). We characterized these puncta using an exon trap line, which tags endogenously expressed Fas2 protein with GFP (Silies and Klämbt, 2010) and which shows the puncta in the same pattern as the Fas2 antibody (Fig. 4, B and C). Using this line, we performed triple stainings with antibodies detecting Fas2 (GFP), endosomes (Rab5), and recycling vesicles (Rab11), which identify only endogenously expressed proteins. This analysis showed many Fas2 puncta that colocalize with one of the two Rab proteins, indicating that Fas2 is endocytosed and recycled at the membrane (Fig. 4, B and C). Fas2 endocytosis was further supported by stainings with a Fas2-specific antibody and overexpressed GFP-tagged Rab5 protein (Fig. 4 A).

To examine whether vesicle trafficking contributes to Fas2 removal from the lateral membrane, we counted the total number of Fas2 puncta and puncta that colocalize either with Rab5 or Rab11 vesicles. We distinguished between egg chambers of three different stages: early follicles that were still round (stage 5/6), oval follicles with no signs of anterior Fas2 disappearance (stage 7), and follicles with cuboidal anterior cells, in which the anterior Fas2 signal starts to disappear (stage 8; Fig. 4 D, pictures). This analysis revealed a continuous increase in the number of Fas2 vesicles between stages 6 and 8 (Fig. 4 D). Moreover, the total number of Fas2-Rab5–positive vesicles per cell increases strongly during this period (Fig. 4 E). Similarly, the proportion of Fas2-Rab5 vesicles in relation to the total number of Rab5 vesicles rises from 3 to 13%, suggesting that an increasing part of the endocytic machinery is engaged in the internalization of Fas2 before stretching occurs (Table S3). We therefore conclude that Fas2 removal from the lateral membrane is mediated by endocytosis.

Fas2 endocytosis is impaired in *Tao* mutant cells

Tao mutant clones exhibit Fas2-positive tubular structures associated with the plasma membrane (Fig. 5 A, arrowheads). These structures are reminiscent of tubules that have been

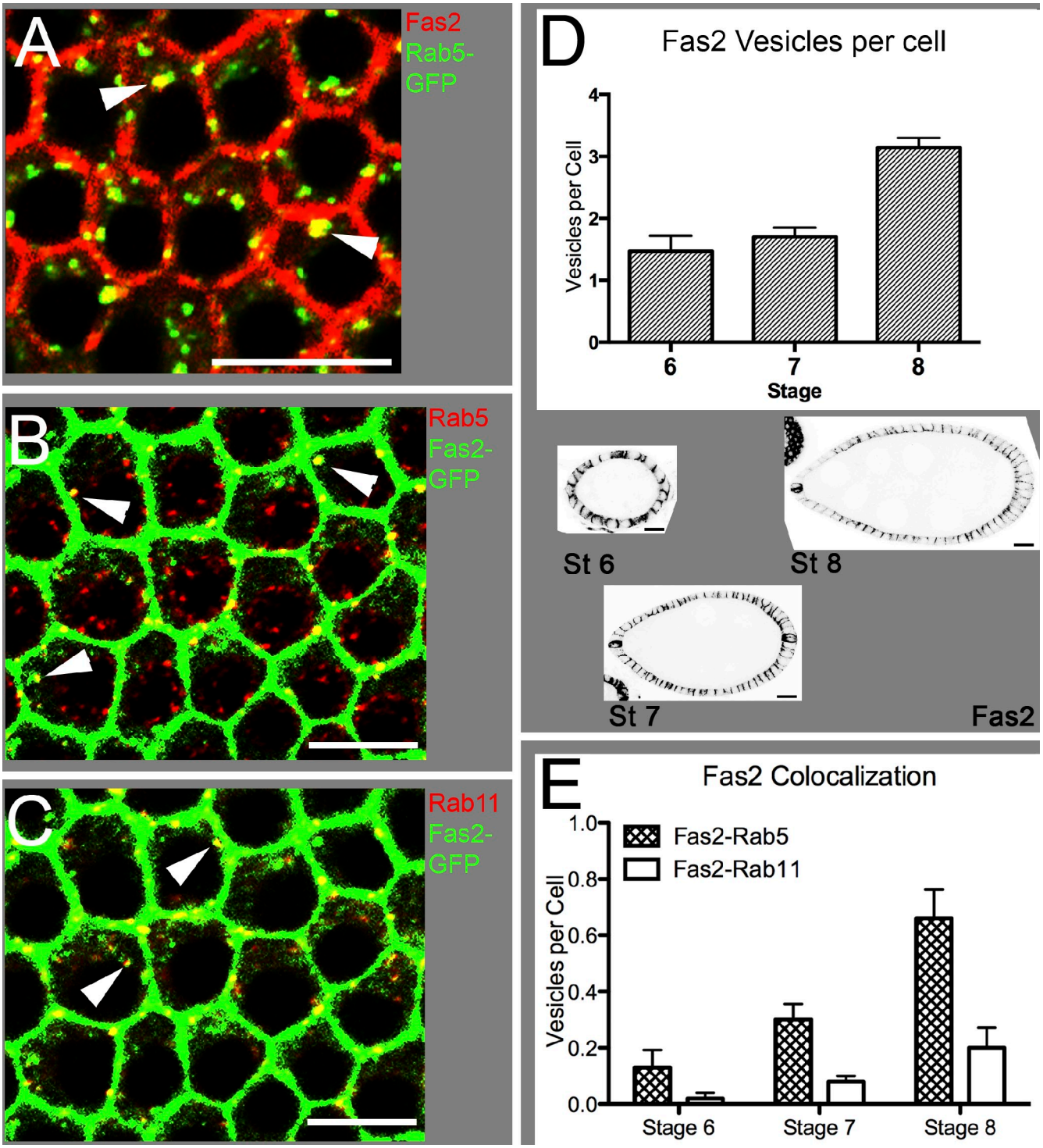

Figure 4. **Cytoplasmic Fas2 puncta colocalize with endosomal and recycling vesicles.** (A–C) Optical confocal sections through the follicular epithelium perpendicular to the apical–basal axis. (A) Double staining with an anti-Fas2 and an anti-GFP antibody detecting *GR1-Gal4*–driven *UAS-Rab5-GFP*. (B and C) Triple staining for Fas2-GFP, Rab5, and Rab11. B shows the Fas2 overlap with Rab5, and C shows the Fas2 overlap with Rab11. Examples of Fas2 vesicles that costain with one of the Rab proteins are marked by arrowheads. (D) Diagram showing Fas2-GFP vesicle numbers at different stages of oogenesis. Bars show the number of Fas2 vesicles counted in optical confocal sections divided by the number of analyzed cells. Below the graph, three follicles are depicted showing examples for the corresponding stages. Error bars indicate standard error. (E) Bars show the number Fas2-GFP vesicles that colocalize with Rab5 and Rab11 during different oogenesis stages. Fas2 vesicles that colocalize with both Rab5 and Rab11 were not included in the diagram. The data shown in D and E summarize the analysis of 15 egg chambers (five for each developmental stage). Processing of the images involved adjustment of γ settings. Error bars indicate standard error. St, stage. Bars, 10 μm.

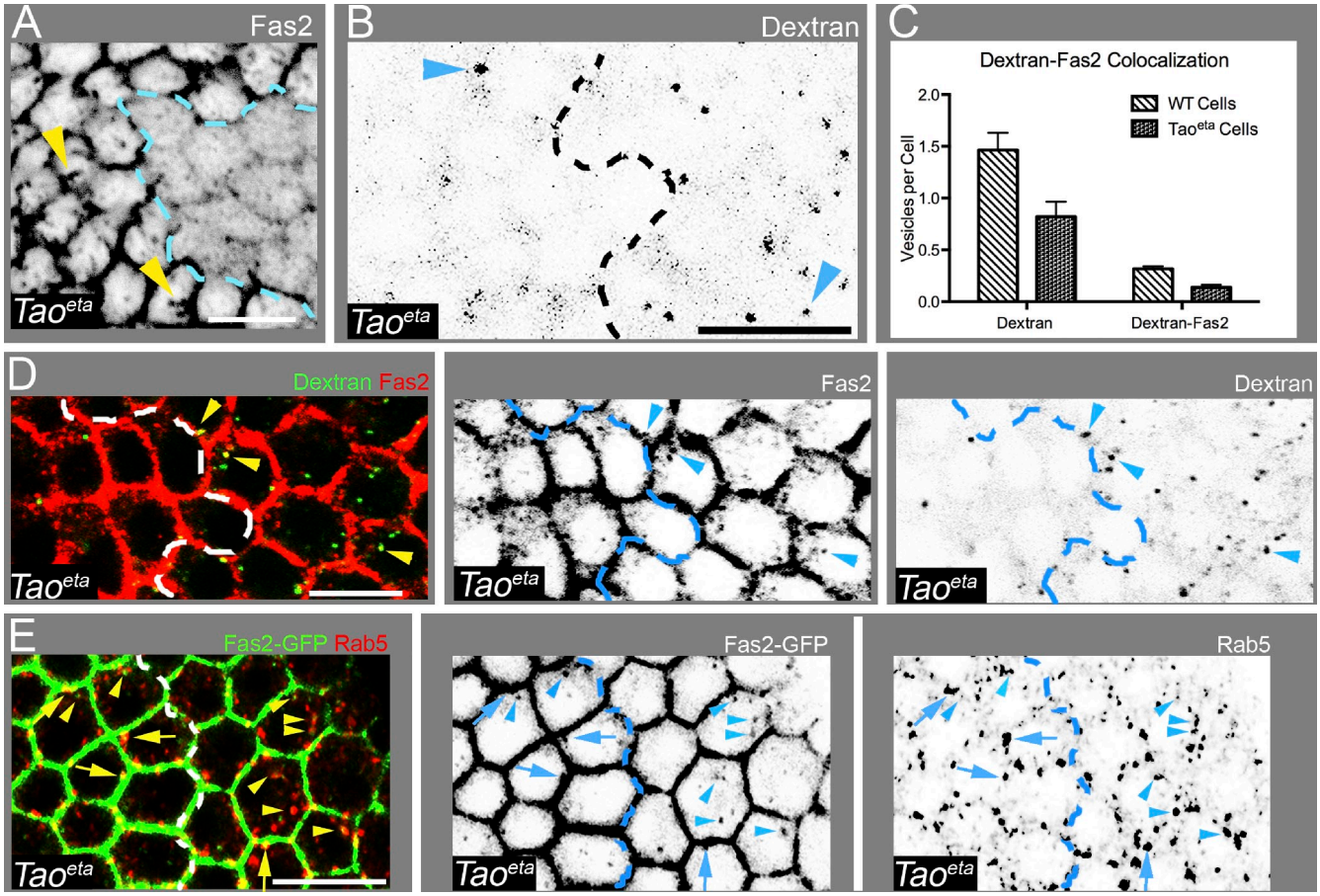

Figure 5. **Fas2 endocytosis is impaired in *Tao* mutant cells.** A, B, D, and E show optical confocal sections perpendicular to the apical–basal axis of the follicular epithelium. (A) *Tao* mutant cell clone (left) stained with an anti-Fas2 antibody showing increased Fas2 levels at the lateral membrane. In addition, tubular Fas2 extensions sprout from the lateral membrane (arrowheads). (B) *Tao* mutant clone in a follicle that has been incubated with fluorescently labeled dextran. Dextran signal is shown in black, and dotted line marks the clone border. Homozygous mutant cells are to the left. Dextran particles that were internalized into follicle cells vary in size. Right arrowhead shows an example for the minimal particle size counted in these experiments. Left arrowhead marks a bigger dextran particle. Analysis of four cell clones generated in three independent uptake experiments revealed a mean reduction of internalized dextran vesicles by 54%. (C) Diagram summarizing the results of three dextran uptake experiments (five clones) in which follicles were subsequently stained for Fas2. Left bars show the total number of dextran vesicles per cell, and right bars show the numbers of cytoplasmic dextran vesicles that colocalize with Fas2. Error bars indicate standard error. A statistical test (*t* two-tailed paired test) was performed to analyze dextran internalization between wild-type (WT) and *Tao* mutant cells ($P = 0.001$) and dextran-Fas2 colocalization ($P = 0.0171$). (D) Follicle with a *Tao* clone incubated in dextran and subsequently stained with an anti-Fas2 antibody. *Tao* mutant cells are left, and wild-type cells are right of the white dotted line. Arrowheads indicate dextran vesicles that colocalize with Fas2. (E) *Tao* mutant cell clone stained for Fas2-GFP and Rab5. *Tao* mutant cells are to the left of the white dotted line. Fas2 and Rab5 channels alone are shown in the right two images. Examples for cytoplasmic Fas2-Rab5 vesicles are marked by arrowheads, whereas membrane-associated vesicular structures are marked by arrows. Processing of the images involved adjustment of γ settings. Blue dotted lines mark the border of the Tao mutant clones. Bars, 10 µm.

described for mutants that affect vesicle scission and endocytosis in the epithelium of the *Drosophila* notum (Georgiou et al., 2008; Leibfried et al., 2008). To test whether *Tao* is required for endocytosis, we performed uptake experiments, in which we incubated mosaic egg chambers with fluorescently labeled dextran. Quantification of dextran vesicle numbers in confocal pictures revealed that dextran internalization is significantly reduced in *Tao* mutant cells compared with neighboring heterozygous cells (Fig. 5 B). We also tested whether this approach monitors Fas2 endocytosis by staining ovaries after dextran incubation with an anti-Fas2 antibody. Notably, many dextran vesicles were Fas2 positive in wild-type cells, indicating that dextran was included in Fas2 endocytotic vesicles (Fig. 5 D, arrowheads). In *Tao* mutant cells, the number of dextran vesicles colocalizing with Fas2 is strongly reduced, indicating that *Tao* is required for efficient Fas2 endocytosis in the follicular epithelium (Fig. 5 C).

To further characterize the endocytosis defect in *Tao* mutants, we quantified the formation of Rab5-positive Fas2 vesicles in homozygous mutant and heterozygous cells. To this end, we recombined the Fas2 exon trap GFP insertion with the Tao^{eta} mutation. To mark cell clones independently of GFP, we generated a P(neoFRT)19A chromosome with a follicle cell–specific enhancer trap, enabling us to detect follicle cell nuclei that are wild type for *Tao* with β-Galactosidase (Müller, 2000). Using these chromosomes, we generated cell clones colabeled for Fas2-GFP and Rab5 and quantified confocal pictures by counting the number of Rab5 vesicles, vesicular Fas2 structures, and their colocalization. Moreover, we determined the subcellular localization of vesicular Fas2-Rab5 structures

Table 1. **Quantification of endocytotic vesicles in *Tao* mutant genetic mosaics**

Genotype	Cytoplasmic Fas2 puncta per cell	Total Rab5 vesicles	Rab5 vesicles within membrane	Membrane-associated Rab5 vesicles		Cytoplasmic Rab5 vesicles	
				+Fas2	−Fas2	+Fas2	−Fas2
$Tao^{eta}/+$	2.16 ± 0.69	12.15 ± 4.13	4.50 ± 1.39	1.55 ± 0.43	0.73 ± 0.20	0.84 ± 0.35	4.53 ± 2.50
Tao^{eta}/Tao^{eta}	2.42 ± 0.52	12.56 ± 3.24	4.38 ± 2.11	2.47 ± 0.73	0.68 ± 0.32	0.39 ± 0.19	4.73 ± 1.30
P-value (*t* test)	0.4884	0.8530	0.9070	0.0278	0.7517	0.0249	0.8666

Confocal pictures of seven stage 8/9 genetic mosaic egg chambers were analyzed, which were stained with GFP to highlight Fas2, Rab5 to mark endosomes, and β-Galactosidase to identify wild-type cells. Total counts of Fas2 puncta per cell reflect only cytoplasmic puncta and do not include plasma membrane–associated structures. Rab5 vesicles are distinguished between vesicles that overlap with the center of the plasma membrane (within membrane), vesicles whose signal overlaps with the plasma membrane but does not touch its center (membrane associated), and vesicles that do not overlap with the plasma membrane (cytoplasmic). Membrane-associated Rab5 vesicles are further distinguished between vesicles that reveal Fas2-positive semicircular or tubular membrane protrusions (+Fas2) and vesicles without such protrusions (−Fas2). *t* test (two-tailed equal variance; $\alpha = 0.05$) was performed to describe the statistical significance of the difference between the values obtained for vesicle numbers in homozygous versus homozygous cell clones.

by distinguishing between cytoplasmic puncta (Fig. 5 E, arrowheads) and semicircular or tubular structures associated with the plasma membrane (Fig. 5 E, arrows). This analysis revealed that in *Tao* mutant cells, plasma membrane–associated Fas2-Rab5 structures were increased, whereas Fas2-Rab5 vesicles in the cytoplasm were reduced (Table 1). The increased accumulation of Fas2-Rab5 structures at the plasma membrane suggests that formation or scission of endocytic Fas2 vesicles is impaired in *Tao* mutant cells. Moreover, it is possible that *Tao* predominantly affects the formation of endocytotic Fas2 vesicles, as the spatial distribution of other (Fas2 negative) Rab5 vesicles was not affected in *Tao* mutant cells. Collectively, these results suggest that Tao activates Fas2 endocytosis by promoting the formation of Rab5 vesicles.

Discussion

Here, we report a novel mechanism regulating the morphogenesis of a squamous epithelium. Our data show that timely controlled removal of the adhesion molecule Fas2 from the lateral membrane is critical for the stretching of cuboidal precursor cells. In this process, Tao initiates morphogenesis by promoting Fas2 endocytosis from the lateral membrane, which reduces adhesive forces and thereby provides plasticity for the cuboidal to squamous cell shape change. Our results are consistent with a model in which homophilic Fas2 interactions act as a glue preventing shortening of the membrane.

A role for *Tao* in promoting endocytosis

Tao function is essential for the process of stretching of epithelial cells. However, our data indicate that *Tao* uses none of its known pathways to control morphogenesis. Similarly, we found no evidence that *Tao* regulates cell stretching via the cytoskeleton. Moreover, our results argue against a role for *Tao* in transcriptional repression of *Fas2*, indicating a function in posttranslational regulation. Indeed, our quantitative analysis of Fas2 vesicles in wild-type follicles indicates that membrane shrinking is initiated by enhanced endocytosis. *Tao* mutant cells have a reduced ability to internalize Fas2 vesicles, contain tubular Fas2 structures typical for endocytosis defects, and show fewer endocytotic Fas2 vesicles in the cytoplasm. This indicates that the overaccumulation of Fas2 at the lateral membrane is caused by defective Fas2 internalization, suggesting a role for *Tao* in promoting endocytosis at the lateral membrane. A similar function of *Tao* in triggering endocytosis of homophilic adhesion proteins has been identified in cultured hippocampal neurons (Yasuda et al., 2007). In contrast to the follicular epithelium, however, *Tao* is acting via the p38 MAP signaling pathway in this cell type.

Tao promotes Fas2 endocytosis not only in the anterior squamous epithelium but acts also in the posterior epithelium, whose cells become columnar by elongating their lateral membrane (Fig. 1, A and H). Although it is surprising that these cells down-regulate a protein that is able to induce cell elongation, it appears that during stage 7/8, all epithelial cells clear their lateral membrane from Fas2 to allow morphogenesis. This suggests that other proteins than Fas2 are responsible for cell elongation in the posterior epithelium.

Is Tao an endocytosis promoter specific for the lateral membrane?

Endocytosis is only impaired but not blocked in *Tao* mutant cells, as they are still able to internalize reduced levels of dextran and Fas2. Consistent with this, the *Tao* phenotype differs from mutants affecting endocytosis in general. Although cell clones mutant for Rab5, the syntaxin family member Avalanche, and Dynamin/Shibire show severe polarity defects and massive overproliferation in the follicular epithelium (unpublished data; Lu and Bilder, 2005), the *Tao* phenotype is restricted to overaccumulation of membrane proteins and cell shape defects. We therefore conclude that *Tao* is not a general endocytosis factor but enhances endocytosis at a critical developmental stage to allow epithelial morphogenesis.

This timely controlled requirement of *Tao* function raises the question whether Tao expression starts just before the onset of morphogenesis or whether the protein is present also in early stages and only activated when Fas2 has to be removed from the lateral membrane. We were unable to detect endogenous Tao protein, as antibodies generated by us and others showed no specific signal in the follicular epithelium. Moreover, analysis of *Tao* mRNA expression does not allow unambiguous conclusions about the onset of *Tao* transcription in the follicular epithelium as a strong signal from the germline cyst covers the signal in the surrounding epithelium.

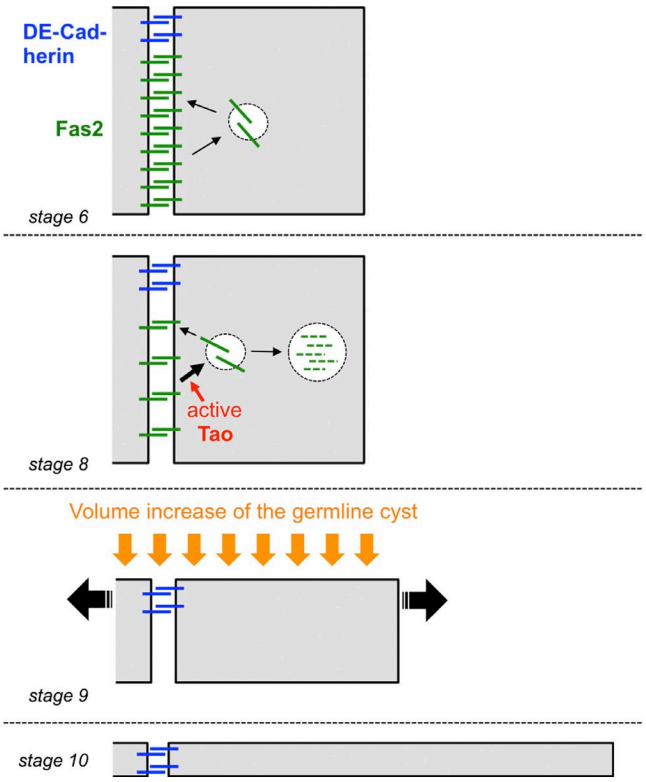

Figure 6. **Model for squamous cell morphogenesis.** See last chapter of the Discussion for explanation.

Using a HA fusion protein, we detected Tao protein at the lateral membrane and in the basolateral cytoplasm of the follicular epithelium. Interestingly, Tao protein accumulation appears as a gradient with the lowest levels in the apical and the highest levels in the basal region of the follicular epithelium (Fig. 1 I). As our rescue experiments demonstrate the functionality of the fusion protein, a gradient of endogenous Tao activity might also exist. This raises the possibility that Tao promotes endocytosis more strongly in basal regions of the lateral membrane. We speculate that there is a switch in Tao activity at the border between the lateral and the basal membrane and that the basal membrane domain is protected from Tao function. A spatial restriction of Tao function to the lateral membrane could be achieved by the localization of a yet unidentified target of Tao kinase. Such a Tao mediator could exclusively localize to the lateral membrane.

The finding that not only Fas2 but also apical and apicolateral proteins, such as DE-cadherin and Crb, overaccumulate in *Tao* mutants might argue against a restriction of Tao function to the lateral membrane. However, in the light of the dramatic change in the geometry of stretching cells, an alternative explanation for the accumulation of these proteins seems more likely. Squamous cell morphogenesis involves a 15-fold surface expansion, which is accompanied by a strong increase in the amounts of proteins determining the apical membrane and forming the adherens junctions. Interestingly, also, posterior cells expand their surface, albeit in less dramatic manner (Kolahi et al., 2009). *Tao* mutant cells are unable to increase their surface area, but they nevertheless produce the same amount of apical and apicolateral proteins, which then concentrate within a restricted area. We therefore propose that the accumulation of Arm, DE-cadherin, and apical proteins in *Tao* mutant cells is not caused by impaired endocytosis but a result of the inability of these cells to increase their surface area. Consistent with this, we found that cells whose stretching is prevented by Fas2 overexpression (and which are wild type for *Tao* function) also concentrate Arm within their restricted apical surface (Fig. 3 E).

A membrane domain–specific endocytosis function for *Tao* is also supported by experiments, which deplete *Fas2* in *Tao* mutant cells. If *Tao* would act all along the plasma membrane, Fas2 removal from the lateral membrane should selectively rescue the lateral defect (i.e., Fas2 accumulation) but should not suppress the accumulation of apical and apicolateral proteins (e.g., Arm). However, *Fas2 Tao* double mutant cells do suppress Arm accumulation (Fig. 2 J). Thus, the primary defect of *Tao* mutants is Fas2 accumulation, which prevents stretching and expansion of the apical surface. The concentration of Arm is only a secondary effect of the cell shape defect. In conclusion, our data favor a model in which Tao promotes endocytosis specifically at the lateral membrane to relieve Fas2-mediated cell adhesion.

The role of *Tao* in squamous cell morphogenesis

The identification of a mechanism initiating epithelial morphogenesis in the follicular epithelium allows us to update the current model of squamous cell morphogenesis in the follicular epithelium. Before morphogenesis, all epithelial cells are cuboidal and adhere apicolaterally via DE-cadherin and more basolaterally via Fas2 interactions. In this period, Fas2 is endocytosed and recycled back to the membrane (Fig. 6, stage 6). Morphogenesis is primed by the Tao kinase, which promotes the endocytosis of Fas2 vesicles. We assume that a large proportion of the Fas2 vesicles enter the lysosomal pathway, leading to Fas2 degradation (Fig. 6, stage 8). The removal of Fas2 from the lateral membrane is a critical first step, which allows morphogenesis to occur. Once Fas2 has disappeared, the cuboidal shape of the epithelial cells is solely stabilized by the zonula adherens. Cell flattening requires a tensile force, and morphometric analysis indicates that this force originates from the continuously growing germline cyst, which stretches cells in the anterior epithelium (Fig. 6, stage 9; Kolahi et al., 2009). Flattening correlates well with the local breakdown of the zonula adherens, suggesting an important role for adherens junctions remodeling in cell stretching (Grammont, 2007). Although the exact molecular mechanism controlling remodeling has still to be elucidated, our data indicate that before cell stretching, lateral cell adhesion has to be reduced to provide morphogenetic plasticity to the lateral membrane.

Given the critical role of *Fas2* down-regulation for epithelial stretching, it is counterintuitive that *Fas2* mutant cells undergo normal morphogenesis. However, a similar scenario has been shown for the morphogenesis of the peripheral nervous system (PNS) in *Drosophila*. Here, Fas2 has to be endocytosed in axons to allow glia cell migration. Despite this important function for Fas2 down-regulation, *Fas2* mutants

show no gross morphological defects in the PNS (Silies and Klämbt, 2010). Thus, although Fas2 down-regulation is critical for epithelial and PNS morphogenesis, both tissues can compensate for the complete loss of the protein. We propose that Fas2 helps to stabilize a morphological state and allows development to proceed only after its timely controlled endocytosis. This mechanism guarantees the correct timing of morphogenesis and thereby helps to coordinate the development of different cell types and tissues. In the follicular epithelium, Fas2 might collaborate with the zonula adherens in counteracting the pressure from the growing germline cyst. As a result, the cuboidal cell shape is stabilized and premature, and uncontrolled stretching is prevented. Subsequently, Fas2 internalization overcomes this control mechanism, and epithelial morphogenesis proceeds.

Materials and methods

Generation of Tao mutants

To generate EMS-induced *Tao* mutants, we made use of an EP element that is inserted into the first, untranslated exon of the Tao locus (EP1455). This transposon neither affects viability nor fertility of the mutant flies. EP elements integrate UAS sequences into the genome, allowing the overexpression of adjacent genes by a Gal4 driver line. Induction of *Tao* expression by combining EP1455 with the ubiquitous driver Tubulin-Gal4 results in lethality. We used this lethal combination of chromosomes to screen for suppressor mutations. To this end, we fed males harboring the EP element with EMS and crossed them to females expressing the Tubulin-Gal4 driver. After screening of more than 10,000 crosses, we obtained 13 suppressors of lethality, which are good candidates to carry mutations in the *Tao* locus. Among those, one suppressor mutation was lethal by itself, which we named Tao^{eta}. Sequence analysis revealed a point mutation in the kinase domain of *Tao*, in which a CAG triplet encoding glutamine (aa 64) is mutated to TAG, resulting in a stop codon.

To generate a deficiency uncovering the *Tao* locus, we used two transposons carrying FRT sites, which allow the recovery of chromosomes with deletions of molecularly defined endpoints (Parks et al., 2004). Following the instructions of Parks et al. (2004), chromosomes harboring the transposons PBac{XP}CG32532^{d02300} and PBac{RB}e01713 were crossed in trans to induce a small deficiency that we named Df(1)14.1 and which uncovers the genes *Grip84*, *carnation*, and *Tao*. The deficiency and the Tao^{eta} allele were recombined with FRT19A to generate genetic mosaic flies (see following paragraph).

Drosophila genetics

Drosophila stocks used were as follows: *yw FRT19A* (Bloomington Stock Center), *w* Tao^{eta} *FRT19A*/FM6, Df(1)14.4 FRT19A/FM6 (both from this work), *w* $Fas2^{eb112}$ FRT19A/FM6 (provided by C. Klämbt, University of Münster, Münster, Germany; Grenningloh et al., 1991), *w ;UAS-Fas2-YFP* (provided by A. Nose, Tokyo University, Tokyo Japan; Kohsaka et al., 2007), *w* $Fas2^{GFP397}$ (exon trap insertion in the Fas2 locus; provided by C. Klämbt), w ;;*UAS-Tao/*TM3 *Sb*, *w ;UAS-HA-Tao/*CyO, *w* $Fas2^{eb112}$ Tao^{eta} *FRT19A/FM6* (all from this work), *GR1-Gal4/*TM3Ser (provided by S. Roth, University of Cologne, Cologne, Germany; Gupta and Schüpbach, 2003), *w ;traffic jam-Gal4/*CyO (provided by J. Brennecke, Institute of Molecular Biotechnology, Vienna, Austria; Olivieri et al., 2010), *w ;;GR1-Gal4 UAS-FLP/*TM3 Ser, *w ;;Kinesin-βGal/*TM3Ser, *w ;;Nod- βGal/* TM3Ser (both provided by S. Roth; Clark et al., 1997), y*w AN365 FRT19A* (recombination of the a follicle cell–specific enhancer trap with FRT19A; the original enhancer trap stock was provided by A. Müller, University of Dundee, Dundee, Scotland, UK), G2H FRT101/FM7, H6 FRT101/FM7 (deletions uncovering *licorn* and *hemipterous*; provided by S. Noselli, University of Nice, Nice, France; Suzanne et al., 1999), and *w ;;*FRT82B $Mpk2^{1}$, *w* $Dsor1^{lh110}$ FRT101/FM7a (both obtained from the Bloomington Stock Center). Strains that were used in RNAi experiments have been provided by the Vienna Drosophila RNAi Center and are listed in Table S1.

Genetic mosaics were generated by using either a heat shock or a UAS/Gal4-inducible Flippase. Heat shock follicle cell clones were induced during prepupae and pupae stages by placing the vials in a 37°C water bath for 1 h for a consecutive 3 d. After eclosion, females were kept at 27°C for 2–3 d and dissected. Alternatively, a UAS-FLP was induced in follicular epithelium using the *GR1-Gal4* driver. To this end, flies were raised at 27°C and, after eclosion, shifted to 29°C for 28–48 h and dissected.

Overexpression of the *UAS-Fas2-YFP* was performed using the *traffic jam-Gal4* driver. Flies were raised at 29°C, and after eclosion, females were kept at 29°C for 3–4 d for dissection.

Antibodies and histology

Ovaries were dissected in S2 medium at RT (PromoCell), fixed for 10 min in 4% formaldehyde, blocked for 30 min in PBS, 0.1% Triton X-100, and 0.1% bovine serum albumin, and incubated with the primary antibodies overnight at RT. For secondary antibodies, a 1-h incubation at 25°C was performed. Finally, ovaries were stained with 0.5 µg/ml DAPI for 15 min, washed, and mounted. See Franz and Riechmann (2010) for a more detailed description.

Primary antibodies used were as follows: rabbit anti-Oskar 1:1,000 (gift from A. Ephrussi, European Molecular Biology Laboratory Heidelberg, Germany), rabbit antiphospho–Histone H3 1:500 (EMD Millipore), mouse anti-Eya (clone eya10H6; Developmental Studies Hybridoma Bank), rabbit antiphospho–Myosin light chain 1:10 (Cell Signaling Technology), mouse anti-Arm 1:200 (clone N2 7A1; Developmental Studies Hybridoma Bank), rat anti–DE-cadherin 1:50 (clone DCAD2; Developmental Studies Hybridoma Bank), rabbit anti-aPKC 1:100 (sc-216; Santa Cruz Biotechnology, Inc.), mouse anti-Dlg 1:50 (clone 4F3; Developmental Studies Hybridoma Bank), rat anti-Crb 1:250 (gift from E. Knust, Max Planck Institute of Molecular Cell Biology and Genetics, Dresden, Germany), rabbit anti-Bazooka 1:250 (gift from A. Wodarz, University of Göttingen, Göttingen, Germany), rabbit anti–Par-6 1:50 (gift from J. Knoblich, Institute of Molecular Biotechnology, Vienna, Austria), mouse anti-Fas2 1:50 (clone 1D4; Developmental Studies Hybridoma Bank), mouse anti-Coracle 1:50 (clone C566.9; Developmental Studies Hybridoma Bank), mouse anti–Fasciclin 3 1:50 (clone 7G10; Developmental Studies Hybridoma Bank), mouse anti–Notch intracellular domain 1:50 (C17.9C6; Developmental Studies Hybridoma Bank), rat anti–α-Tubulin 1:500 (clone YL1/2; AbD Serotec), mouse anti–α-Tubulin 1:50 (DM1A; Sigma-Aldrich), mouse anti–γ-Tubulin 1:200 (GTU-88; Sigma-Aldrich), mouse anti–α-Spectrin 1:50 (3A9; Developmental Studies Hybridoma Bank), mouse anti–β-Galactosidase 1:1,000 (Promega), rabbit anti–β-Galactosidase 1:100 (Invitrogen), rabbit anti-Rab5 1:500 (ab31261; Abcam), mouse anti-Rab11 1:100 (clone 14; BD), anti HA 1:200 (clone 3FC; Roche), rabbit anti-GFP 1:400 (Invitrogen), and goat anti–GFP-FITC 1:200 (GTX26662; GeneTex). Alexa Fluor fluorophore (Alexa Fluor 488, 568, and 647)–coupled secondary antibodies (Invitrogen) were used in a 1:400 dilution. Samples were mounted in Vectashield (Vector Laboratories).

Images were acquired using a confocal microscope (SP5 [Leica] or LSM 700 [Carl Zeiss]) at RT (20–22°C). All pictures were acquired with a 40× (oil immersion) magnification. For the LSM-700, the 40× objective NA is 1.3. For the SP5, the 40× objective NA is 1.25. The pictures were edited, and the figures were assembled with Photoshop (CS3; Adobe).

Generation of UAS-Tao transgenes

mRNA from ovaries was purified using an mRNA isolation kit (µMACS; Miltenyi Biotec) in the fist step for the generation a full-length Tao cDNA. mRNA was used for a reverse transcription reaction with a reverse transcriptase kit (SuperScript III; Invitrogen) and a Tao-specific oligonucleotide (5′-GGGTTGTGTGTCGTGTGTCTTCTTTC-3′) hybridizing with the 3′ untranslated region. With the resulting template and two primers hybridizing with 5′ and 3′ untranslated (5′-CACTGTGTGCTGTGTGAACGTGAAC-3′ and 5′-CACTTGTTGTGGGGGTTGGCATTG-3′) regions of Tao, a PCR reaction was performed. The product was cloned into a cloning kit (pCR TOPO II; Invitrogen) and subsequently sequenced. An EcoR1 fragment containing the full-length open reading frame was subcloned into the pUASp2 vector, and germline transformation was performed using standard protocols. To generate a construct encoding a Tao protein with an N-terminal HA fusion, a PCR fragment containing EcoR1 and Xba1 restriction sites was cloned into a pUASp2 vector containing the HA-encoding sequence.

Quantification of genetic interaction experiments

The quantification of the interaction between the Tao^{eta} allele and knockdown of candidate genes was conducted in stage 9 egg chambers carrying asymmetric clones with respect to the anterior–posterior axis (see Fig. S4). To assess the interaction, the apical–basal cell length of both Tao^{eta} + RNAi and RNAi only (or wild-type control) cells was measured at the level of the nuclei using the confocal microscope (LSM 700) software or ImageJ (National Institutes of Health). The apical–basal length proportion

was calculated between each *Tao*^{eta} + RNAi and RNAi only counterpart. The proportion values obtained from one egg chamber were used to calculate a mean apical–basal length proportion value. The apical–basal length proportion values of four egg chambers were averaged and used to determine whether the *Tao* phenotype was suppressed. Comparison between the candidates' apical–basal length proportion was performed with a one-way analysis of variance and honestly significant difference Tukey's post hoc statistical test.

β-Galactosidase signal intensity measurement

The signal intensity of immunofluorescent β-Galactosidase stainings was measured using ImageJ 1.42j (Mac OS X; Apple). To quantify the signal intensity, the area corresponding to the β-Galactosidase signal within each analyzed cell was selected manually, and its intensity was measured. Measurements of signal intensities were performed with raw confocal pictures. The statistical analysis of *Tao*^{eta}/*Tao*^{eta} versus *Tao*$^{+}$/*Tao*$^{+}$ data were performed with a *t* nonpaired two-tailed nonequal variance test.

Vesicle number and vesicle colocalization quantification

For wild-type follicles, puncta counted within one follicle were added and divided by the number of analyzed cells. We considered puncta that are distinguishable from the background and not linked to the membrane signal. To quantify the colocalization between Fas2, Rab5, and Rab11, 10 cells per follicle were selected in the midanterior follicular epithelium. Subsequently, Fas2 vesicles that colocalized with Rab5 or Rab11 within the selected cells were counted. For each follicle, the number of Fas2-Rab5– or Fas2-Rab11–colocalizing vesicles was added and divided by the number of cells analyzed.

To quantify the colocalization between Fas2 and Rab5 in the *Tao* mutant genetic mosaics, three categories of puncta were distinguished: Fas2-GFP-Rab5–positive structures embedded within the membrane, Fas2-GFP-Rab5–positive tubular structures that protrude from the plasma membrane (Fas2-GFP-Rab5 membrane associated), and Fas2-GFP-Rab5–positive vesicles in the cytoplasm. The statistical analysis of Fas2-GFP-Rab5 colocalization for the three categories, between *Tao*^{eta} homozygous and *Tao*^{eta} heterozygous cells, was performed with a *t* nonequal variance test. The criteria used to count a colocalization event as positive were that 50% or more of the Fas2 structure colocalized with Rab5 or Rab11.

Dextran uptake assay

Ovaries were dissected in S2 medium and immediately transferred to a 0.6 mM dextran (fluorescein labeled, lysine fixable, 3,000 molecular weight; Molecular Probes) solution (S2 medium supplemented with 10% fetal bovine serum) for 3 min at 25°C in a thermomixer (450 rpm). Subsequently, the ovaries were washed with 1 ml PBS and fixed in 4% formaldehyde in PBS for 10 min. Staining procedures were performed as described in Antibodies and histology. To assess dextran-Fas2 colocalization, the Fas2 antibody was used at a 1:25 dilution. To quantify the dextran uptake in the *Tao* mutant genetic mosaics, the total number of dextran vesicles within the wild-type and *Tao* mutant clone was quantified and averaged by the number of cells analyzed within each clone. To quantify the dextran-Fas2 colocalization, the total number of dextran-Fas2–colocalizing vesicles was counted in the wild-type and mutant clones (only the cytoplasmic Fas2 signal was considered). The total number of dextran-Fas2 vesicles was averaged by the number of cells analyzed within each clone. The statistical analysis of *Tao* versus wild-type cells was performed with a *t* two-tailed paired test.

Statistical analysis

The dataset analysis was performed in Excel 2008 (Microsoft) for Mac OS X (v12.2.0) and Prism 5 (GraphPad Software) for Mac OS X (v5.0d). For all statistical tests, the significance level was set at $\alpha = 0.05$.

Online supplemental material

Fig. S1 shows the process of epithelial stretching in wild-type follicles. Fig. S2 shows exclusion of possible Tao functions and pathways during oogenesis. Fig. S3 shows that *Tao* function is not mediated via the cytoskeleton. Fig. S4 explains how the anterior–posterior length proportion was determined. Fig. S5 shows the expression of a reporter for Fas2 transcription. Table S1 lists candidates tested in the *Tao* interaction screen. Table S2 shows quantification of β-Galactosidase signal intensities in wild-type and homo- and heterozygous *Tao* mutant cell clones. Table S3 shows quantification of Fas2, Rab5, and Rab11 puncta and their subcellular distribution in wild-type egg chambers. Online supplemental material is available at http://www.jcb.org/cgi/content/full/jcb.201207150/DC1.

We thank V. Benecke for generating the *Tao*^{eta} allele and S. Költzer for generating transgenic flies. We thank C. Klämbt, E. Kunst, A. Wodarz, J. Knoblich, A. Müller, B. Baum, S. Noselli, A. Matsumoto, M. Gonzalez-Gaitan, A. Nose, A. Ephrussi, J. Brennecke, the Vienna Drosophila RNAi Center, and the Bloomington Stock Center for reagents and fly stocks. Support by F. Bestvater and the German Cancer Research Center Light Microscopy Facility is gratefully acknowledged. We thank S. Roth, T. Vaccari, M. Carl, and N. Berns for comments on the manuscript.

This work was supported by grants (Sonderforschungsbereich 572, project B9, and Sachmittelbeihilfe) of the German research council and a fellowship from the Medical Faculty Mannheim to J.M. Gomez.

Submitted: 24 July 2012
Accepted: 20 November 2012

References

Baum, B., and M. Georgiou. 2011. Dynamics of adherens junctions in epithelial establishment, maintenance, and remodeling. *J. Cell Biol.* 192:907–917. http://dx.doi.org/10.1083/jcb.201009141

Boggiano, J.C., P.J. Vanderzalm, and R.G. Fehon. 2011. Tao-1 phosphorylates Hippo/MST kinases to regulate the Hippo-Salvador-Warts tumor suppressor pathway. *Dev. Cell*. 21:888–895. http://dx.doi.org/10.1016/j.devcel.2011.08.028

Clark, I.E., L.Y. Jan, and Y.N. Jan. 1997. Reciprocal localization of Nod and kinesin fusion proteins indicates microtubule polarity in the *Drosophila* oocyte, epithelium, neuron and muscle. *Development*. 124:461–470.

Deng, W.M., C. Althauser, and H. Ruohola-Baker. 2001. Notch-Delta signaling induces a transition from mitotic cell cycle to endocycle in *Drosophila* follicle cells. *Development*. 128:4737–4746.

Franz, A., and V. Riechmann. 2010. Stepwise polarisation of the *Drosophila* follicular epithelium. *Dev. Biol.* 338:136–147. http://dx.doi.org/10.1016/j.ydbio.2009.11.027

Georgiou, M., E. Marinari, J. Burden, and B. Baum. 2008. Cdc42, Par6, and aPKC regulate Arp2/3-mediated endocytosis to control local adherens junction stability. *Curr. Biol.* 18:1631–1638. http://dx.doi.org/10.1016/j.cub.2008.09.029

Grammont, M. 2007. Adherens junction remodeling by the Notch pathway in *Drosophila melanogaster* oogenesis. *J. Cell Biol.* 177:139–150. http://dx.doi.org/10.1083/jcb.200609079

Grenningloh, G., E.J. Rehm, and C.S. Goodman. 1991. Genetic analysis of growth cone guidance in *Drosophila*: fasciclin II functions as a neuronal recognition molecule. *Cell*. 67:45–57. http://dx.doi.org/10.1016/0092-8674(91)90571-F

Gupta, T., and T. Schüpbach. 2003. Cct1, a phosphatidylcholine biosynthesis enzyme, is required for *Drosophila* oogenesis and ovarian morphogenesis. *Development*. 130:6075–6087. http://dx.doi.org/10.1242/dev.00817

Harris, T.J. 2012. Adherens junction assembly and function in the *Drosophila* embryo. *Int. Rev. Cell Mol. Biol.* 293:45–83. http://dx.doi.org/10.1016/B978-0-12-394304-0.00007-5

Harris, T.J., and U. Tepass. 2010. Adherens junctions: from molecules to morphogenesis. *Nat. Rev. Mol. Cell Biol.* 11:502–514. http://dx.doi.org/10.1038/nrm2927

Horne-Badovinac, S., and D. Bilder. 2005. Mass transit: epithelial morphogenesis in the *Drosophila* egg chamber. *Dev. Dyn.* 232:559–574. http://dx.doi.org/10.1002/dvdy.20286

Hutchison, M., K.S. Berman, and M.H. Cobb. 1998. Isolation of TAO1, a protein kinase that activates MEKs in stress-activated protein kinase cascades. *J. Biol. Chem.* 273:28625–28632. http://dx.doi.org/10.1074/jbc.273.44.28625

King, I., L.T. Tsai, R. Pflanz, A. Voigt, S. Lee, H. Jäckle, B. Lu, and U. Heberlein. 2011. *Drosophila tao* controls mushroom body development and ethanol-stimulated behavior through *par-1*. *J. Neurosci.* 31:1139–1148. http://dx.doi.org/10.1523/JNEUROSCI.4416-10.2011

Kohsaka, H., E. Takasu, and A. Nose. 2007. In vivo induction of postsynaptic molecular assembly by the cell adhesion molecule Fasciclin2. *J. Cell Biol.* 179:1289–1300. http://dx.doi.org/10.1083/jcb.200705154

Kolahi, K.S., P.F. White, D.M. Shreter, A.K. Classen, D. Bilder, and M.R. Mofrad. 2009. Quantitative analysis of epithelial morphogenesis in *Drosophila* oogenesis: New insights based on morphometric analysis and mechanical modeling. *Dev. Biol.* 331:129–139. http://dx.doi.org/10.1016/j.ydbio.2009.04.028

Laprise, P., and U. Tepass. 2011. Novel insights into epithelial polarity proteins in *Drosophila*. *Trends Cell Biol.* 21:401–408. http://dx.doi.org/10.1016/j.tcb.2011.03.005

Leibfried, A., R. Fricke, M.J. Morgan, S. Bogdan, and Y. Bellaiche. 2008. *Drosophila* Cip4 and WASp define a branch of the Cdc42-Par6-aPKC pathway regulating E-cadherin endocytosis. *Curr. Biol.* 18:1639–1648. http://dx.doi.org/10.1016/j.cub.2008.09.063

Levayer, R., and T. Lecuit. 2012. Biomechanical regulation of contractility: spatial control and dynamics. *Trends Cell Biol.* 22:61–81. http://dx.doi.org/10.1016/j.tcb.2011.10.001

Liu, T., J.L. Rohn, R. Picone, P. Kunda, and B. Baum. 2010. Tao-1 is a negative regulator of microtubule plus-end growth. *J. Cell Sci.* 123:2708–2716. http://dx.doi.org/10.1242/jcs.068726

López-Schier, H., and D. St Johnston. 2001. Delta signaling from the germ line controls the proliferation and differentiation of the somatic follicle cells during *Drosophila* oogenesis. *Genes Dev.* 15:1393–1405. http://dx.doi.org/10.1101/gad.200901

Lu, H., and D. Bilder. 2005. Endocytic control of epithelial polarity and proliferation in *Drosophila. Nat. Cell Biol.* 7:1232–1239. http://dx.doi.org/10.1038/ncb1324

Meignin, C., I. Alvarez-Garcia, I. Davis, and I.M. Palacios. 2007. The salvador-warts-hippo pathway is required for epithelial proliferation and axis specification in *Drosophila. Curr. Biol.* 17:1871–1878. http://dx.doi.org/10.1016/j.cub.2007.09.062

Müller, H.A. 2000. Genetic control of epithelial cell polarity: lessons from *Drosophila. Dev. Dyn.* 218:52–67. http://dx.doi.org/10.1002/(SICI)1097-0177(200005)218:1<52::AID-DVDY5>3.0.CO;2-L

Olivieri, D., M.M. Sykora, R. Sachidanandam, K. Mechtler, and J. Brennecke. 2010. An in vivo RNAi assay identifies major genetic and cellular requirements for primary piRNA biogenesis in *Drosophila. EMBO J.* 29:3301–3317. http://dx.doi.org/10.1038/emboj.2010.212

Parks, A.L., K.R. Cook, M. Belvin, N.A. Dompe, R. Fawcett, K. Huppert, L.R. Tan, C.G. Winter, K.P. Bogart, J.E. Deal, et al. 2004. Systematic generation of high-resolution deletion coverage of the *Drosophila melanogaster* genome. *Nat. Genet.* 36:288–292. http://dx.doi.org/10.1038/ng1312

Polesello, C., and N. Tapon. 2007. Salvador-warts-hippo signaling promotes *Drosophila* posterior follicle cell maturation downstream of notch. *Curr. Biol.* 17:1864–1870. http://dx.doi.org/10.1016/j.cub.2007.09.049

Poon, C.L., J.I. Lin, X. Zhang, and K.F. Harvey. 2011. The sterile 20-like kinase Tao-1 controls tissue growth by regulating the Salvador-Warts-Hippo pathway. *Dev. Cell*. 21:896–906. http://dx.doi.org/10.1016/j.devcel.2011.09.012

Pope, K.L., and T.J. Harris. 2008. Control of cell flattening and junctional remodeling during squamous epithelial morphogenesis in *Drosophila. Development*. 135:2227–2238. http://dx.doi.org/10.1242/dev.019802

Raman, M., S. Earnest, K. Zhang, Y. Zhao, and M.H. Cobb. 2007. TAO kinases mediate activation of p38 in response to DNA damage. *EMBO J.* 26:2005–2014. http://dx.doi.org/10.1038/sj.emboj.7601668

Riechmann, V., and A. Ephrussi. 2004. Par-1 regulates *bicoid* mRNA localisation by phosphorylating Exuperantia. *Development*. 131:5897–5907. http://dx.doi.org/10.1242/dev.01515

Sato, K., Y. Hayashi, Y. Ninomiya, S. Shigenobu, K. Arita, M. Mukai, and S. Kobayashi. 2007. Maternal Nanos represses hid/skl-dependent apoptosis to maintain the germ line in *Drosophila* embryos. *Proc. Natl. Acad. Sci. USA*. 104:7455–7460. http://dx.doi.org/10.1073/pnas.0610052104

Shulman, J.M., R. Benton, and D. St Johnston. 2000. The *Drosophila* homolog of *C. elegans* PAR-1 organizes the oocyte cytoskeleton and directs *oskar* mRNA localization to the posterior pole. *Cell*. 101:377–388. http://dx.doi.org/10.1016/S0092-8674(00)80848-X

Silies, M., and C. Klämbt. 2010. APC/C(Fzr/Cdh1)-dependent regulation of cell adhesion controls glial migration in the *Drosophila* PNS. *Nat. Neurosci.* 13:1357–1364. http://dx.doi.org/10.1038/nn.2656

St Johnston, D., and B. Sanson. 2011. Epithelial polarity and morphogenesis. *Curr. Opin. Cell Biol.* 23:540–546. http://dx.doi.org/10.1016/j.ceb.2011.07.005

Suzanne, M., K. Irie, B. Glise, F. Agnès, E. Mori, K. Matsumoto, and S. Noselli. 1999. The *Drosophila* p38 MAPK pathway is required during oogenesis for egg asymmetric development. *Genes Dev.* 13:1464–1474. http://dx.doi.org/10.1101/gad.13.11.1464

Szafranski, P., and S. Goode. 2004. A Fasciclin 2 morphogenetic switch organizes epithelial cell cluster polarity and motility. *Development*. 131:2023–2036. http://dx.doi.org/10.1242/dev.01097

Tanentzapf, G., C. Smith, J. McGlade, and U. Tepass. 2000. Apical, lateral, and basal polarization cues contribute to the development of the follicular epithelium during *Drosophila* oogenesis. *J. Cell Biol.* 151:891–904. http://dx.doi.org/10.1083/jcb.151.4.891

Timm, T., X.Y. Li, J. Biernat, J. Jiao, E. Mandelkow, J. Vandekerckhove, and E.M. Mandelkow. 2003. MARKK, a Ste20-like kinase, activates the polarity-inducing kinase MARK/PAR-1. *EMBO J.* 22:5090–5101. http://dx.doi.org/10.1093/emboj/cdg447

Tomancak, P., F. Piano, V. Riechmann, K.C. Gunsalus, K.J. Kemphues, and A. Ephrussi. 2000. A *Drosophila melanogaster* homologue of *Caenorhabditis elegans par-1* acts at an early step in embryonic-axis formation. *Nat. Cell Biol.* 2:458–460. http://dx.doi.org/10.1038/35017101

Wang, Y., and V. Riechmann. 2007. The role of the actomyosin cytoskeleton in coordination of tissue growth during *Drosophila* oogenesis. *Curr. Biol.* 17:1349–1355. http://dx.doi.org/10.1016/j.cub.2007.06.067

Xu, T., and G.M. Rubin. 1993. Analysis of genetic mosaics in developing and adult *Drosophila* tissues. *Development*. 117:1223–1237.

Yasuda, S., H. Tanaka, H. Sugiura, K. Okamura, T. Sakaguchi, U. Tran, T. Takemiya, A. Mizoguchi, Y. Yagita, T. Sakurai, et al. 2007. Activity-induced protocadherin arcadlin regulates dendritic spine number by triggering N-cadherin endocytosis via TAO2beta and p38 MAP kinases. *Neuron*. 56:456–471. http://dx.doi.org/10.1016/j.neuron.2007.08.020

Zarnescu, D.C., and G.H. Thomas. 1999. Apical spectrin is essential for epithelial morphogenesis but not apicobasal polarity in *Drosophila. J. Cell Biol.* 146:1075–1086. http://dx.doi.org/10.1083/jcb.146.5.1075